Originally published as:

The M_w 8.1 2014 Iquique, Chile, seismic sequence: a tale of foreshocks and aftershocks

S. Cesca,[1] F. Grigoli,[2,3] S. Heimann,[1] T. Dahm,[1,2] M. Kriegerowski,[2] M. Sobiesiak,[4] C. Tassara[5] and M. Olcay[5]

[1]*GFZ German Research Center for Geosciences Potsdam, D-14467 Potsdam, Germany. E-mail* simone.cesca@gfz-potsdam.de
[2]*University of Potsdam, D-14476 Potsdam, Germany*
[3]*OGS, I-34010 Sgonico (Trieste), Italy*
[4]*Christian-Albrechts-University Kiel, D-24118 Kiel, Germany*
[5]*Universidad Nacional Arturo Prat, Arturo Prat Chacón 2120, Iquique, Chile*

SUMMARY

The 2014 April 1, M_w 8.1 Iquique (Chile) earthquake struck in the Northern Chile seismic gap. With a rupture length of less than 200 km, it left unbroken large segments of the former gap. Early studies were able to model the main rupture features but results are ambiguous with respect to the role of aseismic slip and left open questions on the remaining hazard at the Northern Chile gap. A striking observation of the 2014 earthquake has been its extensive preparation phase, with more than 1300 events with magnitude above M_L 3, occurring during the 15 months preceding the main shock. Increasing seismicity rates and observed peak magnitudes accompanied the last three weeks before the main shock. Thanks to the large data sets of regional recordings, we assess the precursor activity, compare foreshocks and aftershocks and model rupture preparation and rupture effects. To tackle inversion challenges for moderate events with an asymmetric network geometry, we use full waveforms techniques to locate events, map the seismicity rate and derive source parameters, obtaining moment tensors for more than 300 events (magnitudes M_w 4.0–8.1) in the period 2013 January 1–2014 April 30. This unique data set of fore- and aftershocks is investigated to distinguish rupture process models and models of strain and stress rotation during an earthquake. Results indicate that the spatial distributions of foreshocks delineated the shallower part of the rupture areas of the main shock and its largest aftershock, well matching the spatial extension of the aftershocks cloud. Most moment tensors correspond to almost pure double couple thrust mechanisms, consistent with the slab orientation. Whereas no significant differences are observed among thrust mechanisms in different areas, nor among thrust foreshocks and aftershocks, the early aftershock sequence is characterized by the presence of normal fault mechanisms, striking parallel to the trench but dipping westward. These events likely occurred in the shallow wedge structure close to the slab interface and are consequence of the increased extensional stress in this region after the largest events. The overall stress inversion result suggests a minor stress rotation after the main shock, but a significant release of the deviatoric stress. The temporal change in the distribution of focal mechanisms can also be explained in terms of the spatial heterogeneity of the stress field: under such interpretation, the potential of a large megathrust earthquake breaking a larger segment offshore Northern Chile remains high.

Key words: Earthquake source observations; South America.

1 INTRODUCTION

On 2014 April 1, at 23:46:49.9 UTC the M_w 8.1 Iquique earthquake struck offshore Northern Chile at 70.73° Lon. W, 19.59° Lat. S and at 34 km depth (GEOFON catalogue). This earthquake partially filled the known Northern Chile seismic gap, which lasted 137 yr since the 1877 M_w 8 Iquique earthquake (Nishenko 1985; Lomnitz 2004; Metois *et al.* 2013). The main shock was followed on 2014 April 3, by a large aftershock (M_w 7.6), whose epicentre was located about 110 km SSE of the main shock. A first analysis

of the rupture process of the main shock and its largest aftershock have been discussed in Schurr *et al.* (2014), using a combination of GPS, accelerometer and broad-band data. Results indicated that the rupture areas broken by these earthquakes had an overall length of about 150–200 km, and only affected the central part of the former seismic gap. For both earthquakes, the rupture nucleated at shallow depth and propagated downdip, towards a region of higher locking. Hayes *et al.* (2014) relocated and derived source models for the main shocks and a subset of the foreshocks and aftershocks. Both studies agreed that the potential for further large megathrust earthquakes in Northern Chile remains high, and that the 2014 sequence only released a part of the accumulated strain. A striking observation on the 2014 Iquique earthquake sequence is the increase in seismic activity, which took place in the months prior to the main shock (Ruiz *et al.* 2014). However, the potential triggering role played by the foreshock is still debated (Bürgmann 2014; Ruiz *et al.* 2014; Schurr *et al.* 2014). In particular, it remains controversial whether the deformation data confirm that the foreshock seismicity was accompanied by aseismic slip (Bürgmann 2014), with different studies assigning the surface displacements measured by GPS during the foreshocks time mostly to the foreshock activity (Schurr *et al.* 2014; Bedford *et al.* 2015) or strongly involving an aseismic slow slip process (Ruiz *et al.* 2014). A slow slip was independently supported by Kato & Nakagawa (2014) and Meng *et al.* (2015), upon the detection of repeating events and the observation of episodes of slow epicentral migration. The interpretation of foreshock seismicity and aseismic slip at the Iquique rupture area has important implications towards the assessment of future rupture scenarios offshore Northern Chile. According to Schurr *et al.* (2014), the slip deficit at the rupture area of the 2014 sequence was only partially reduced, decreasing the probability of a large future earthquake along the former gap, but not implying that this region will act as a barrier for future large earthquakes. If, in change, the surface displacement was larger and mostly accommodated through a slow aseismic slip (Ruiz *et al.* 2014), the estimated slip deficit would be smaller and future rupture scenarios could more likely affect shorter segments towards north, in the Arica region and/or south, between the rupture area of the 2014 Iquique and 2007 Tocopilla earthquakes.

The availability of more than 150 earthquakes with magnitude above M_L 4 (GEOFON catalogue) in the epicentral region (here 22°–18° Lat. S, 68°–72° Lon. W, depths shallower than 80 km) from 2013 January 1 until 2014 March 31 (the day before the main shock), and the large aftershock sequence, provides an excellent data set to study the temporal variation of seismicity parameters. The aim of this paper is to evaluate spatial and temporal changes of seismic source parameters, with a particular interest towards the comparison of foreshocks and aftershocks focal mechanisms. Through this analysis, we first aim to evaluate whether seismic source parameters showed a significant temporal variation throughout the earthquake preparatory phase, and discuss the possible information provided by the foreshock activity. Foreshock sequences have been analysed for several earthquakes (e.g. Jones & Molnar 1976; Kanamori 1981; Dodge *et al.* 1995; Helmstetter & Sornette 2003; Mignan 2012) and their prognostic information investigated. If a foreshock model can be confirmed, a relatively long precursory phase could help to mitigate earthquake risk at plate boundaries. An anomalous foreshock activity, preceding a large earthquake has been considered either as a consequence of a triggering process or to be correlated to the tectonic loading (Mignan 2014, and references therein). More specifically, it is possible to distinguish among rupture nucleation models where the foreshocks are the localized expression of asperities failures accompanying an aseismic nucleation process,

and those where foreshocks are responsible of a stress change triggering a runaway process culminating in the main shock (Dodge *et al.* 1996). Bouchon *et al.* (2013) distinguished foreshock patterns prior to interplate and intraplate large earthquakes, showing that many large earthquakes at the plate interface are preceded by an accelerating foreshock activity, which can last days to months. The observation of more frequent foreshocks at plate boundaries was used there to support the aseismic nucleation model, where foreshocks are the result of asperities breaking accompanying slow slip on a broader area, which precedes the interface rupture through a large earthquake. The comparison of foreshocks and aftershocks focal mechanisms should also help to evaluate a possible coseismic rotation of the stress tensor, as observed for larger earthquakes (Hardebeck 2012), or to discuss the spatial stress heterogeneity and its temporal evolution. Following a similar approach, we aim to quantify and assess the robustness of stress rotation to infer the amount of the pre-main shock deviatoric stress relieved by the main shock stress drop, which is important to judge future earthquake scenarios at the Northern Chile seismic gap.

2 PREVIOUS SEISMICITY AND DATA OVERVIEW

Large intraplate megathrust events are common at the western margin of the Southamerican plate. Their occurrence is driven by the subduction of the oceanic Nazca plate, with a convergence of about 6.7 cm y^{-1} (Norabuena *et al.* 1998; Schurr *et al.* 2012). Megathrust earthquakes in this region can occur both offshore and onshore, and typically at shallow depths of less than 60 km, with a high tsunami potential. The size and rate of seismicity, including the 1960 M_w 9.5 Chile earthquake, the largest earthquake ever recorded, pose Chile among the most highly seismogenic regions worldwide (Lomnitz 2004). The large Northern Chile seismic gap is defined based on events with $M > 8$, as the most recent ones took place in 1868 (Arica earthquake, M 8.5–9.1) and 1877 (Iquique earthquake, M 8–8.8). They were located offshore the cities of Arica and Iquique, upon which they are named (Lomnitz 2004, and references therein). Since little information is known for these earthquakes, their hypocentral locations, sizes and magnitudes have strong uncertainties, which can amount up to 0.5 magnitude order (Comte & Pardo 1991; Lomnitz 2004). Both earthquakes generated strong tsunamis and had rupture lengths exceeding 400 km (Dorbath *et al.* 1990). The occurrence of a very large earthquake in the region previous to the 1868/1877 earthquakes is dated to 1604, with an intervent time gap of almost 300 yr, compatible, for example, to central Chile (Dura *et al.* 2015). Since 1900, six additional significant events (1905, 1906, 1911, 1933, 1945, 1956) with $M_s > 7$ and estimated lengths of 38–77 km took place in the gap, also in the vicinity of the epicentral location of the 2014 Iquique earthquake; additional smaller events (M_s 5.8–6.9) in the years 1967–1971 were discussed by Malgrange & Madariaga (1983). The largest one (M_s 7.6) on 1933 February 23 (Comte & Pardo 1991) mostly affected the city of Iquique. Even considering significant uncertainties for the 1933 earthquake, its reported location (Centennial catalogue; Engdahl & Villaseñor 2002) and size (length ∼80 km; Comte & Pardo 1991) suggest its rupture could correspond to the main slip patch of the recent 2014 Iquique earthquake; this would support a scenario of repeated rupture of the same main asperity. The comparable location of the 1933 earthquake is also confirmed by its consequences, with the seismological bulletin of the astronomical observatory in La Plata, Argentina, reporting that the event 'was felt in the

saltpeter region and in the sea in front of Iquique by the ship Caulin' (http://storing.rm.ingv.it/bulletins/ISC-GEM).
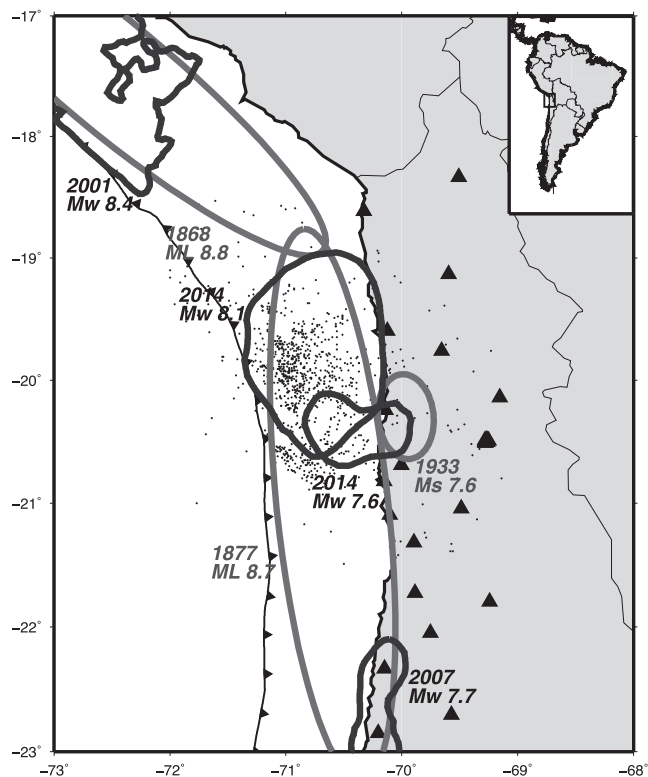
In the last two decades, the seismic gap was located in the area which has been hypothesized as the rupture area of the 1877 earthquake, which extends for about 500 km approximately in the latitude range 18.5–22.0° Lat. S. The segment to the south was broken in the last two decades by the 1995 M_w 8.0–8.1 Antofagasta (Ruegg *et al.* 1996; Delouis *et al.* 1997; Sobiesiak 2000) and the 2007 M_w 7.7–7.8 Tocopilla earthquakes (Delouis *et al.* 2009; Schurr *et al.* 2012). The segment to the north, which has a different NW-SE orientation following the bending on the trench northwards of the Northern Chile gap, was broken in 2001 by the Arequipa (Southern Peru) earthquake (Bilek & Ruff 2002; Pritchard *et al.* 2007). Southwards, the Antofagasta and Tocopilla earthquakes have a similar thrust fault geometry, striking almost NS, with a 17°–20° dipping angle and a rake of 97°–110°, indicating a minor oblique component. The Arequipa earthquake (Bilek & Ruff 2002) had a similar geometry, except for its NW-SE striking. These three earthquakes provide important references for the analysis of the 2014 Iquique earthquake and its seismic sequence, because they occurred along neighbouring slab segments, had comparable magnitudes, shallow depths and thrust mechanisms.

The instrumentation of the Integrated Plate boundary Observatory in Chile (IPOC; Schurr *et al.* 2009) provides a dense regional seismological network. In particular, we rely on the broad-band instrument of the IPOC network (GFZ German Research Centre for Geosciences & Institut des Sciences de l'Univers-Centre National de la Recherche CNRS-INSU 2006) for the analysis of source processes of moderate earthquakes at regional distances. For larger earthquakes (i.e. above M 5.5), we rely on the Global Seismological Network, due to saturation problems at regional broad-band sensors. Fig. 1 illustrates the seismic gap, the rupture of significant previous earthquakes prior to the Iquique earthquake and the location of available broad-band stations from the IPOC initiative, at the time of the seismic sequence, between 2013 January and 2014 April.

3 SPATIOTEMPORAL PATTERNS OF FORESHOCKS AND AFTERSHOCKS

Since 2013, the slab segment offshore Northern Chile comprised between 21° and 19° Lat. S was affected by significant seismicity episodes at the plate interface. A first small sequence was observed in 2013 summer, culminating in an M_L 6.1 event on 2013 August 5. A second increment of seismicity, taking place during the first days of 2014 January (M_L 6.1 on 2014 January 4, M_L 6.3 on 2014 January 8), affected a southern region, close to the epicentre of the 2014 April 3, M 7.6 aftershock. Since the middle of March, the seismicity drastically increased in a third, more important sequence. The maximal magnitude observed in previous months was trespassed again on 2014 March 16, with an M_L 6.9 event, followed by at least seven more earthquakes with magnitude larger than M_L 6.0, until 2013 March 25. Finally, a more quiet period of few days preceded the occurrence of the main shock, on April 1, with a magnitude M_w 8.1.

In this work, we perform different cluster analysis to investigate and compare foreshocks and aftershocks. The clustering procedure relies on a density based approach (Cesca *et al.* 2014; Maghsoudi *et al.* 2014). The method searches for highly populated regions, and defines the cluster edges where the earthquake density drops below a chosen threshold. Earthquakes not reachable through a densely populated path do not belong to any cluster and are treated as outliers. We use an evolution of the focal mechanism clustering

Figure 1. The former Northern Chile seismic gap, with the rupture areas of the 2014 Iquique M_w 8.1 and 7.6 earthquakes, largest earthquakes in the last two decades (black solid lines), and of significant historical earthquakes (grey solid lines); the location of the 1933 earthquake is set according to the Centennial catalogue (Engdahl & Villaseñor 2002), its size according to Comte & Pardo (1991). The maps shows the location of available broad-band stations from the IPOC initiative (triangles) and the observed seismicity with $M_L \geq 4.0$ in the time period from 2013 January 1 to 2013 April 30 (GEOFON catalogue, black dots represent seismicity at less than 60 km depth, grey dots deeper events).

algorithm by Cesca *et al.* (2014), and perform the clustering to separately assess the similarity among hypocentral locations, origin times and focal mechanisms.

For the spatial clustering, where the distance between two earthquakes is simply the Euclidean distances between their hypocentres, we consider 3033 $M_L \geq 3.0$ earthquakes from the GEOFON catalogue (http://geofon.gfz-potsdam.de/eqinfo/list.php) in the period 2013 January 1–2014 April 30, located in the region comprised between 21.5° and 18.5° Lat. S, 69.5 and 72.0° Lon. W, and at less than 100 km depth. The chosen time frame provides comparable populations of foreshocks (1347) and aftershocks (1685). We choose the clustering parameters ($\varepsilon = 0.10$, $N_{min} = 25$, see Cesca *et al.* 2014) to minimize the number of unclustered events while resolving main clusters structures. Beside the uncertainties in locations, three clusters are resolved (Fig. 2). The recognition of these spatial clusters has been confirmed independently using different seismic catalogues, such as the one provided online by the Chilean National Seismological Centre. The two most populated red and blue clusters correspond to the region where the main shock and the largest M_w 7.6 aftershock nucleated, respectively. According to finite source modelling results by Schurr *et al.* (2014), both these events propagated downdip and towards the low seismicity region between the two main clusters. Finally a smaller (green) cluster is located north of the main one. The comparison of foreshock and aftershock distributions (Fig. 2) shows that the spatial extension of the region
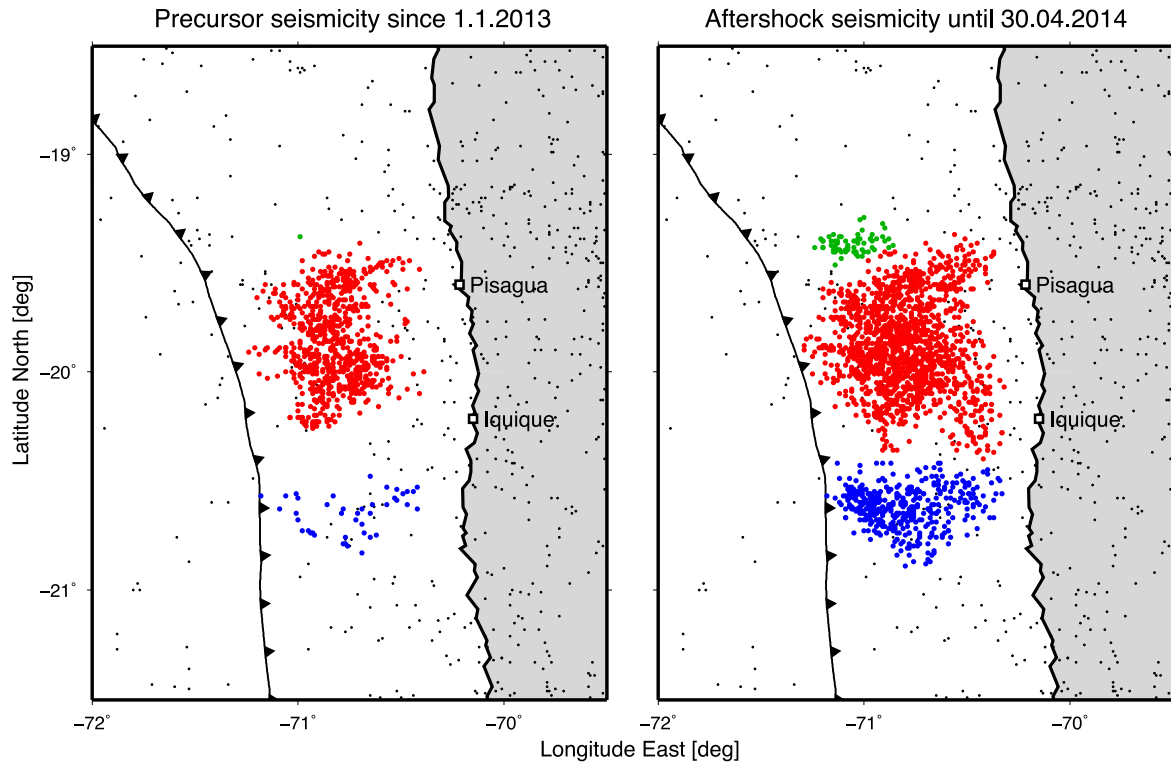
Figure 2. Comparison of foreshock and aftershock seismicity in the former Northern Chile seismic gap based on the GEOFON catalogue, limited to events shallower than 100 km depth, from 2013 January 1 until the 2014 April 1, M_w 8.1 Iquique earthquake (a) and from that earthquake until 2014 April 30 (b). Colours correspond to identified spatial clusters: Pisagua cluster (red), Iquique cluster (blue) and small Northern cluster (green). Black dots correspond to unclustered events.

affected by the aftershock activity (at least during 2014 April) could have already been guessed by the foreshocks distribution. A second important observation is that foreshocks and aftershocks are mostly localized at shallow depths, whereas the rupture areas associated to the two largest events on April 1 and 3 extended further down the slab (Schurr *et al.* 2014).

We analyse the temporal evolution of the seismic sequence by considering seismicity rates and maximal magnitudes (Fig. 3), and compare the temporal evolution of the Iquique sequence to those of previous large events in the broader area of Northern Chile and Peru (the 1995 Antofagasta, the 2001 Arequipa and the 2007 Tocopilla earthquakes). The remaining gaps to the north and south of the area affected by the 2014 Iquique sequence can be well depicted in this figure. The foreshock activity preceding the Iquique earthquake is outstanding compared to these reference cases: it is characterized by a long-lasting activity, with a peak magnitude escalation during the last few weeks preceding the main shock, with no equivalent in any of the three prior sequences here considered for comparison, nor in the case of the recent 2015 Illapel, Chile, earthquake. Although a foreshock activity over years was also observed for the Antofagasta earthquake (Delouis *et al.* 1997), it was not comparable to the Iquique case in terms of peak magnitudes and acceleration of moment release. An anomalous foreshock activity in the region of Iquique is also mentioned in the historical seismic bulletin of the seismological observatory in Toronto, Canada, at more than 7000 km distance (the bulletin archived by the International Seismological Centre is accessible at: http://storing.rm.ingv.it/bulletins/ISC-GEM), during the last two weeks preceding the 1933 M_s 7.6 earthquake, whose location, given the obvious uncertainties, could well correspond to the area of the

2014 Iquique sequence. Analogical records from seismological observatories at closer distance, if available, could be used in future to support this information.

4 LOCATION AND SEISMICITY RATES

In order to study changes in seismicity pattern and rate, we relocated 436 seismic events above M_L 4.0 occurred from 2013 January 1 to 2014 April 30. Despite the dense network, its geometry and the lack of ocean bottom seismometer (OBS) stations at the time of the sequence limits the resolution of standard location techniques. Therefore, we used a method designed to locate hypocentres and map the seismicity rate, by modifying a waveform stacking method proposed by Grigoli *et al.* (2014). This method is based on stacking STA/LTA traces of specific characteristic functions at different recording stations along theoretical *P* and *S* traveltime surfaces corresponding to a hypothetical source location. The method requires no phase picking and no phase association. Iterating this process for different source locations for a 3-D grid containing the whole seismogenic volume, we can obtain a spatial coherence matrix whose maximum corresponds with the location of the seismic event. To locate earthquakes, we rely on broad-band recordings from the IPOC regional seismic network, which includes 19 broad-band seismic stations deployed in the Chilean territory. The location procedure was performed by scanning a spatial grid of 600 km × 600 km × 225 km (east–west, north–south and depth range) with a spacing of 3 km. Theoretical traveltimes have been computed for a 1-D velocity model, extracted from the CRUST2.0 database (Bassin *et al.* 2000). We successfully located the complete data set by using the waveform
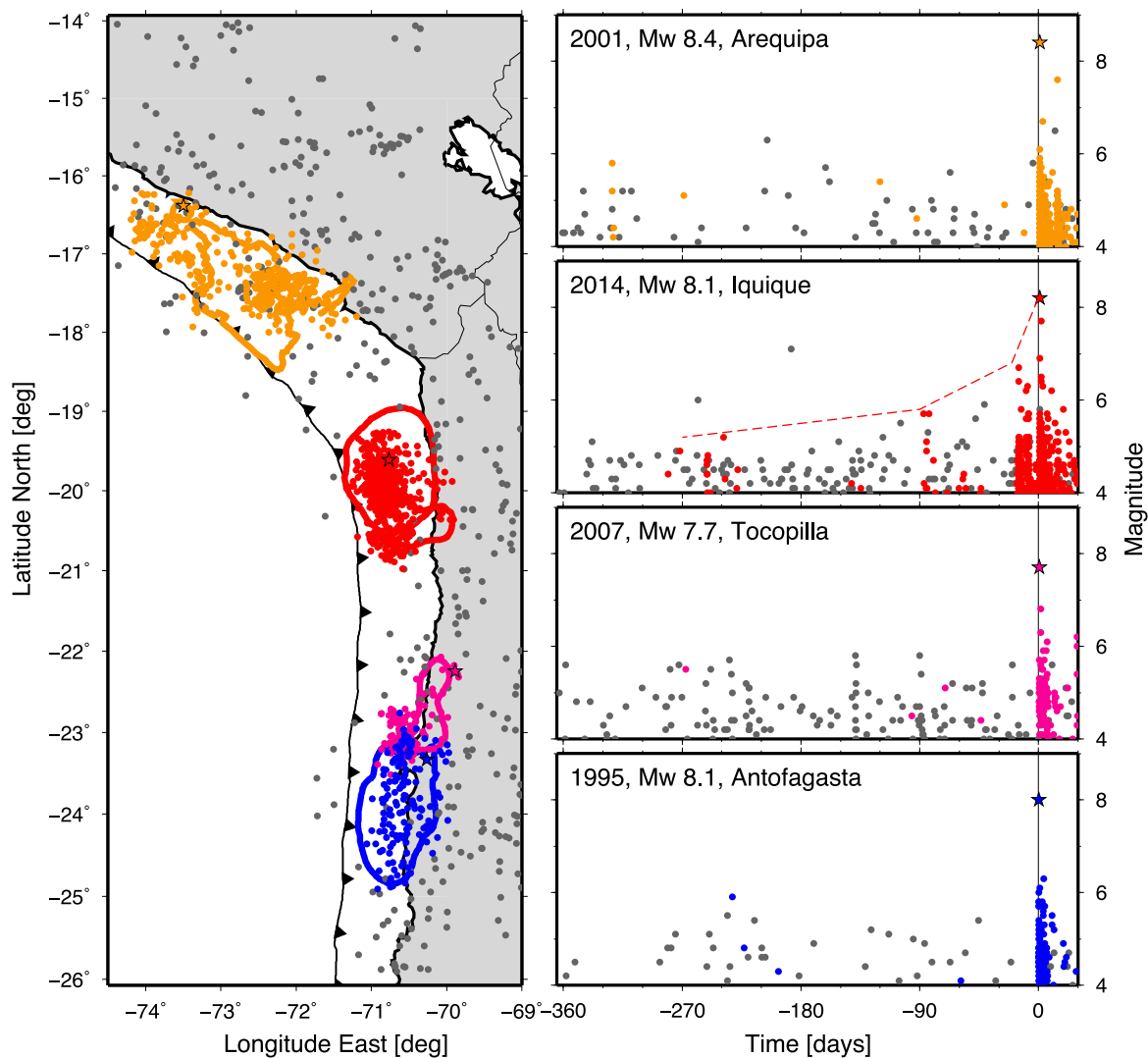
Figure 3. Spatial and temporal clusters, comparing the Iquique sequence to large thrust earthquakes in Southern Peru and Northern Chile in the last 20 yr (1995 Antofagasta, 2001 Arequipa, 2007 Tocopilla earthquakes). Left: the map illustrates the spatiotemporal clusters corresponding to the four seismic sequences, each denoted by a different colour; rupture areas (coloured lines) for the main shocks (stars) are plotted after Pritchard *et al.* (2007) and Schurr *et al.* (2012, 2014); foreshocks and aftershocks (coloured circles) are plotted for a period of one year preceding the main quake and 30 d after it (spatially unclustered events in the considered earthquake regions and time spans are plotted as grey circles). Right: temporal evolution of seismicity and magnitudes of foreshocks (events occurring in the rupture area during the year preceding the main quake) and aftershock (in the same area, in the following 30 d), which highlights the anomaly of the foreshock activity preceding the 2014 Iquique earthquake; the timing of the earthquake is identified by a vertical line and by the reference time on the timescale (expressed in days with respect to the origin time). Events are sorted upon their location from north to south.

stacking location method. Fig. 4 shows two examples of the spatial coherence matrices related to two single event locations of the catalogue (the 2014 January 12, 14:52, M_L 4.1 foreshock and the April 3, 15:43, M_L 4.2, aftershock). In both cases, the spatial coherence matrices show a clear maximum corresponding with the modeled earthquake hypocentral region.

The location procedure provides a 3-D mapping of the coherence value (Grigoli *et al.* 2013). In this paper, we further exploit the information of the coherence matrix on both the hypocentral location and its uncertainty. We consider a broader region to ensure that all locations are well confined within the tested grid. Each event coherence matrix is normalized with respect to its hypervolume, so that the integral of the coherence along the full grid is equal to 1. Multiple normalized coherence matrices are stacked to highlight the seismicity distribution for consecutive time periods, with the advantage that location uncertainties are fully considered. To this purpose, we first

stack the coherence matrices for all events in a given time range. The resulting matrix describes the spatial distribution of seismicity; it is useful to interpret data set with large location uncertainties, since these can be directly considered in a probabilistic framework (Drew *et al.* 2013). Examples of such graphical representations are given in Fig. 5, where estimated seismicity distributions for different time frames of the sequence are compared, together with vertical E–W cross-sections. The first time frame (Fig. 5a) refers to the considered foreshock activity, with seismic events since 2013 January 1, until the main shock on 2014 April 1. The second and third time frames (Figs 5b and c) are related to the days immediately after the main shock and the largest aftershock (2014 April 3), respectively. Finally, Fig. 5d is dedicated to the following aftershock sequence, in the time frame from 2014 April 5 to 30. The analysis of these plots point out that most of the foreshock activity was concentrated in a segment comprised among 19.4° and 20.4° Lat. S, covering
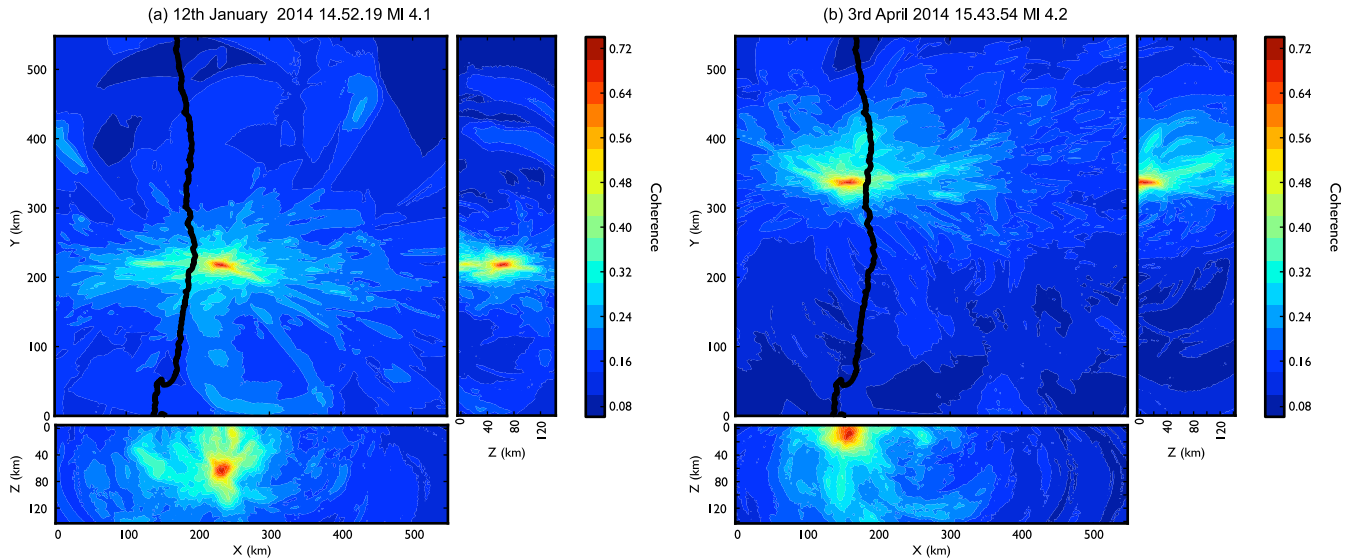
Figure 4. Spatial coherence matrices related to two events of the catalogue: the 2014 January 12, 14:52, M_L 4.1 (left) and the April 3, 15:43, M_L 4.2, (right). Coherence matrix *XY* is obtained by projecting, for each *X–Y*, its maximum along *Z* (coherence matrices *XZ* and *YZ* are obtained in a similar way). Coherence values are represented in colour scale. The origin of the reference system has coordinate: Lat. S 23.5° and Lon. W 72.0°.
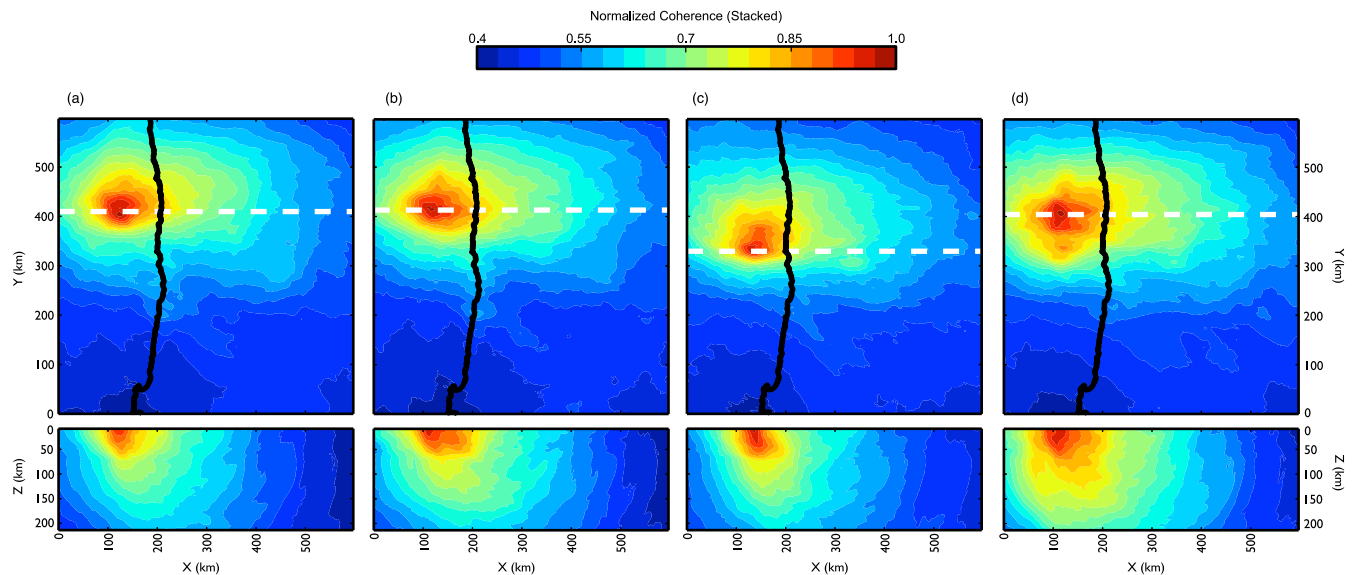
Figure 5 Spatiotemporal evolution of the seismicity in the study area, divided in four consecutive time frames (epicentral maps only): (a) seismic events occurred since 2013 January 1 and until 2014 April 1, day of occurrence of the main shock, (b) time span between the main shock and the largest aftershock, (c) time span from the largest aftershock until 2014 April 5, (d) later aftershock seismicity, from 2014 April 5 until April 30. Upper plots show the stacked coherences on a horizontal projections, bottom plots their E–W cross-sections in correspondence to the maximal coherence (dashed white lines).

the same region where the main shock nucleated, and where first aftershocks were observed. The first activity in the Iquique cluster, observed in 2014 January (see Fig. 2), is comparatively much weaker, and therefore not depicted in the plot. The region of highest seismicity rate strongly migrated southward to the Iquique patch (20.4°–20.9° Lat. S) in the early days following the 2014 April 3, M_w 7.6 earthquake, and spread to the broader area comprising both patches in the later aftershock sequence from April 5 on.

5 MOMENT TENSORS AND CENTROID LOCATIONS

Hayes *et al.* (2014) have first provided moment tensor (MT) solutions for largest foreshocks and aftershocks of the Iquique sequence,

revealing a dominance of thrust fault mechanisms. Whereas most mechanisms are striking parallel to the slab orientation, some shallow events show a significant rotation (about 60°–70°) and strike NW-SE, including one of the largest foreshock (*M* 6.7, 2013 March 16). Here we extend the MT analysis by a double couple (DC) and full MT inversion of a broader data set of 333 earthquakes, for the time period 2013 January 1–2014 April 30, obtaining MTs and centroid locations down to a magnitude M_w 4.0.

We model full waveform displacement traces and amplitude spectra at regional distances and follow a multistep inversion algorithm (Cesca *et al.* 2010, 2013) based on the Kiwi tools software (Heimann 2011, http://kinherd.org). As a result, we obtain DC and full MT source models, centroid location and depth, scalar moment and moment magnitude. In this work we perform the regional MT in-

version by fitting displacement traces in the time domain. Waveforms and metadata have been downloaded from IRIS and GEOFON repositories for broad-band stations up to a distance of 400 km from the starting epicentral location. Original traces were corrected for the instrumental response, integrated to displacements, filtered in the frequency band 0.01–0.03 Hz, tapered according to the epicentral distance and decimated to 2 Hz. The inversion is performed iteratively for 196 starting source configuration, inverting seismic source parameters while allowing for the alignment of synthetic and observed seismograms, by minimizing the L2 norm misfit among time traces. The MT inversion is combined with a dense grid search in the space of latitude, longitude, depth and centroid time, in order to improve the centroid location and depth estimate and the centroid time. Inversion results have been manually controlled and the inversion procedure repeated after excluding problematic (e.g. noise or tilt affected) traces. Synthetic seismograms have been computed upon a Green's function database, which was built using a reflectivity code (QSEIS; Wang 1999) for a 1-D velocity model built using the same local crustal model used for the full waveform location and an AK135 mantle model. Finally, only best results, below the chosen misfit threshold, are considered for further interpretation. In this way, we could obtain 326 regional MTs, out of the 436 tested events, with the remaining lower quality solutions mainly corresponding to events occurring in the coda of larger events (e.g. during the first three days of April, where seismograms were contaminated by the signals of the main shock and its largest aftershocks).

For few larger events, with magnitudes above M 5.5, we relied on teleseismic recordings. Teleseismic inversions have been also performed using the Kiwi tools, but following a slightly different scheme, and relying on bodywave recordings (fitting 60 s long displacement data of vertical P and horizontal S components, filtered with a four poles Butterworth filter between 0.01 and 0.05 Hz). The first inversion step, fitting amplitude spectra in the frequency domain is carried out to identify a set of well matching source model configurations. These are used in the second inversion step to perform a time-domain inversion; note that the inversion is non-linear also in the time domain, since we use an L1 norm and resolve for source parameters and centroid location. From each starting solutions, the inversion is performed by a gradient search method to minimize the L1 norm misfit between observed and synthetics displacement traces. Uncertainties are estimated for all source parameters through a bootstrap approach, by simulating multiple random stations configurations. The teleseismic inversion follows the procedure used in the routine MT inversion of the Kinherd project (Heimann 2011).

The resulting catalogue includes 335 MTs (Fig. 6), for events with moment magnitude down to M_w 4.0 (the two largest events are widely discussed in early publications, for example, by Schurr *et al.* 2014; Hayes *et al.* 2014 and Ruiz *et al.* 2014). Out of these, we have 128 solutions for foreshocks of the 2014 April 1 event (since 2013 January 1) and 206 solutions for its aftershocks (until 2014 April 30). Our results indicate that non-DC components were in general not significant, either because of their negligible size, or because full MT solutions were not improving the misfit significantly, compared to DC ones. Therefore, we only discuss here DC solutions. In most cases focal mechanisms are characterized by thrust mechanisms, with a low-angle eastward dipping fault plane. A smaller population of normal faulting is also observed, as well as few other mechanisms associated to crustal faults inland. Centroid depths along different cross-sections (Fig. 6, bottom) show that most events are confined at the slab interface. However, the seismicity is partially diffuse with some centroid depths extending in the upper wedge. This concerns both events located along the shallower western part of the slab

segment, in agreement with Ruiz *et al.* (2014), and those located more to the east, where the slab deepens and normal faulting are mostly observed.

The distribution of focal mechanisms is discusses using a focal mechanism clustering algorithm (Cesca *et al.* 2014), where we use the Kagan angle (Kagan 1991) as metric. The clustering algorithm is first used to automatically classify the events and to identify clusters of events with similar mechanisms. In a second stage, we use the algorithm to evaluate the average mechanism in each cluster, with the aim of investigating weak spatial and temporal changes in the clusters average focal mechanisms during the foreshock and aftershock sequences and in different spatial clusters; this information will be used at a later stage to assess potential spatial and temporal stress changes. The results of the clustering algorithm (Fig. 7) confirm the dominance of thrust mechanisms both in the foreshock and aftershock sequence. Whereas a single cluster of thrust mechanisms well samples the rupture geometry of the events in the foreshock sequence, during the aftershock sequence smaller populations of weaker normal and vertical faulting are additionally observed. The orientation of thrust mechanisms well matches the slab geometry, striking parallel to the trench and with a low-angle dip towards east. Normal-faulting aftershocks have a similar striking, but their lower angle plane dip westward. In the western section of the slab, thrust events are more diffused, and some occurs in the overriding plate, including few thrust events with different orientations (see also Ruiz *et al.* 2014; Schurr *et al.* 2014). In the deeper eastern section, thrust events are confined close to the slab, while normal faulting are more scattered. Our depth analysis suggests they occur close above the slab interface. Representative focal mechanisms for each cluster can be found by minimizing the cumulative Kagan angle distance to the cluster population, either scanning the entire space of focal mechanism orientations, or only searching among mechanisms corresponding to the earthquake data set. In our case both approaches lead to very similar estimates, and therefore we only discuss results of the latter approach. The difference among average mechanisms obtained for the Pisagua (strike 8°, dip 19°, rake 114°) and Iquique (strike 16°, dip 20°, rake 122°) clusters is minor, considering the distribution of mechanisms in both patches. Similarly, the average mechanisms obtained for the foreshock (strike 3°, dip 21°, rake 111°) and aftershock (strike 8°, dip 23°, rake 112°) sequence are comparable. These results indicate that the rupture process along the slab is consistent and homogeneous in the different spatial patches along the slab and remain unchanged during the time preceding and following the main shock. The absence of significant changes in the different thrust mechanisms families finally suggests the lack of spatial or temporal variation of the slip vector, and thus of the direction of the shear stress.

In order to further investigate possible depth differences among normal and thrust faulting earthquakes, and in order to judge how separated they may be in depth, we carefully analyse to two selected earthquake (Fig. 6), which took place close offshore Iquique on 2014 April 5 and 11, and are characterized by a common centroid locations and magnitude (about M_w 5), but different focal mechanisms: the first event has a standard thrust mechanism, oriented consistently with the slab and a centroid depth of 25 km. The second event pertains to the normal-faulting cluster and has a centroid depth of 20 km. In order to independently assess the depth of these two events, we model their velocity waveforms at station PB06, which is located at about 295 km epicentral distance towards SSE. Records at this station were chosen because they nicely show multiple onsets, which result from its favourable distance and azimuth in combination to the source radiation patterns. In particular,
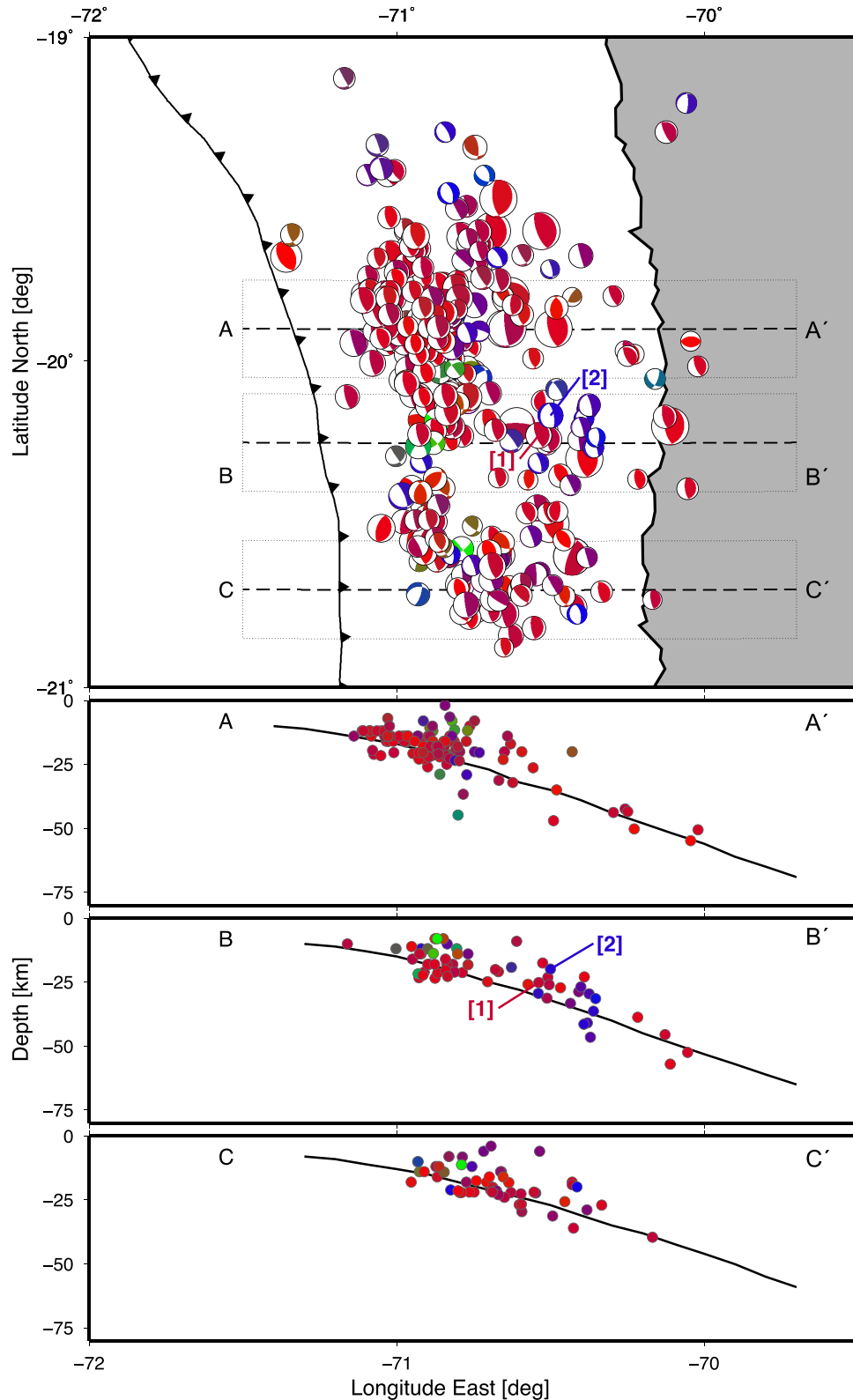
Figure 6. Pure DC moment tensor results based on the inversion of regional and teleseismic data. The size of the focal sphere is scaled with the magnitude, the colour is chosen based on the source type classification by Frohlich (1992): red is used for thrust faulting, blue for normal faulting, green for strike-slip. The map view plot (top) shows that seismicity is dominated by thrust mechanisms, with additional normal faulting, mostly concentrated in the northernmost part and in the easternmost part of the cloud, among the two main seismicity patches. Few strike-slip mechanism are resolved for secondary faults inland. The depth distribution (bottom) is shown for three vertical E-W cross-sections (AA′ through the northern Pisagua cluster, BB′ through a normal fault area, CC′ through the southern Iquique cluster). The depth difference of one thrust and one normal-faulting event with similar magnitude and location (denoted with [1] and [2] both in the map view and BB′ cross-section) is further investigated using an alternative array-based technique, in order to independently confirm that normal faulting occur above the slab interface. Slab geometry at different cross-sections was derived upon Hayes *et al.* (2012).
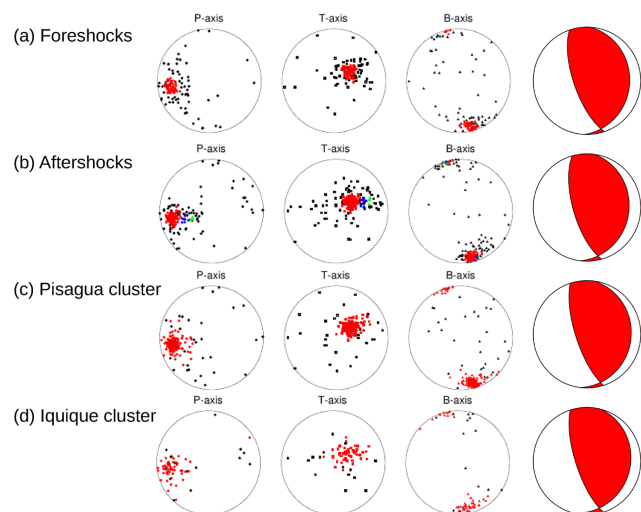
Figure 7. Overview of the focal mechanism clustering result. Focal mechanisms are plotted by means of the orientation of the pressure (*P*), tension (*T*) and null axis (*B*) for all foreshocks (a), all aftershocks (b), the events in the Pisagua spatial cluster (c) and in the Iquique spatial cluster (d). Colours are used to denote the clustered events; the focal sphere corresponding to the mean focal mechanism of each cluster is plot on the right side.

vertical component velocity signals show a low amplitude first *P* onset followed by an energetic pulse, which can be modeled by a *P* wave reflected at the sea floor. Modelling of these waveforms and the temporal offset of these phases allow a more precise resolution of the hypocentral depth, since the delay between the *P* onset and the sea bottom reflection is directly controlled by the source depth. Fig. 8 illustrates the results of our analysis. Beside the observation of nicely anticorrelated waveforms, which confirms the similarity of locations and difference in the focal mechanisms, the onset delays of about 4.5 s are only reproducible, in both cases, for a common source depth of 19 km, slightly above the slab interface. These results confirm the depth similarity among the events and further reduce the minor (5 km) depth difference resolved by the centroid location procedure; they proof that the two earthquakes with different rupture mechanisms must have occurred within a reduced seismogenic volume.

6 STRESS INVERSION

Assuming that rupture occurs on pre-existing planes of weaknesses, with a slip in the direction of the maximal shear stress resolved on the plane, the orientation of the principal stresses and the relative stress magnitude can be inferred (Gephart & Forsyth 1984). Different methods for stress inversion have been proposed (e.g. Michael 1984, 1987; Gephart & Forsyth 1984; Gephart 1990; Angelier 2002), which all assume a homogeneous stress field over the spatial-temporal range of the ensemble of input focal solutions (see e.g. Maury *et al.* 2013 for recent applications). The method employed in our study is an in-house developed inversion based on the minimization of the radiated seismic energy. It has been successfully tested against the methods by Michael (1984) and Gephart & Forsyth (1984), and was applied to different data sets from Germany and the Czech Republic (Reinhardt 2007). Input is the DC components of the MTs of the foreshock (125 events) and aftershock activity (201 events).

Results are plotted in Fig. 9 and indicate for foreshocks an azimuth and plunge orientation of the maximum compressive stress

(σ_1) as 254°/26° and for the least compressive stress (σ_3) as 70°/64°. This stress orientation slightly rotates during the aftershock sequence to values as 260°/32° (σ_1) and 65°/60° (σ_3). The shape of the stress tensor is in both cases represented by $R = 0.5$. The rotation of the stress tensor from the pre-seismic to the early (based on one month aftershock) post-seismic phase in terms of Kagan angles is about 6° around a near-horizontal σ_2 axis (Fig. 9). The sense of the rotation is as found by Hardebeck (2012) for larger thrust earthquakes (e.g. Maule, Tohoku), where the rotation angle could rise up to 30°. We attribute the smaller magnitude of the rotation angle to the fact that the overall magnitude of the Pisagua earthquake, and therefore its slip magnitude and the size of the fault plane, are much smaller in comparison to Tohoku and Maule.

7 DISCUSSION

The foreshock sequence preceding the Iquique earthquake was for many reasons unusual, if compared to similarly large thrust earthquakes affecting the neighbouring slab sections offshore Northern Chile and Southern Peru in the last 20 yr, and offers a unique opportunity to investigate spatial and temporal evolution of focal mechanisms. According to observed data, early foreshocks may be dated at least to 2013 summer, almost one year before the occurrence of the 2014 April 1, M_w 8.1 Iquique earthquake. Short seismicity episodes in 2013 summer and 2014 January were substituted by a runaway process during the last and most significant phase of the foreshock activity in 2013 March, where the increasing seismicity rate was accompanied by an increase of peak magnitudes. Although not observed for recent earthquakes on neighbouring segments, such acceleration of seismicity rate and moment release was often observed for interplate percursors. Bouchon *et al.* (2013) confirmed that, in most cases, there was a high probability that such pattern was not due to a chance. The temporal evolution of the foreshock sequence of the Iquique earthquake has also been discussed by Kato & Nakagawa (2014), who recognized a slow migration of foreshocks towards the region where the M_w 8.1 nucleated, and by Schurr *et al.* (2014), who modeled temporal changes in seismicity rates and *b*-values using an Epidemic-Type-Aftershock-Sequence model, suggesting that the observed alternated sequence of seismic quiescence and recovery background seismicity phases is an indicator for local stress accumulation. One of the most striking feature of the foreshock activity is its spatial location, with hypocentres remaining confined mostly within two main clusters, which location and extension reflects both the locations and size of the two main events (2014 April 1 and 3) and of the following aftershock activity.

The role of foreshocks in the triggering of the main shock has been first debated by Schurr *et al.* (2014) and Ruiz *et al.* (2014). The localized occurrence of foreshocks within spatial clusters located in correspondence to low coupling regions (Béjar-Pizarro *et al.* 2013; Metois *et al.* 2013) supports a scenario of aseismic slow slip at the Pisagua and Iquique patches during the foreshock sequence, with the foreshocks hypocentres clustering at the location of asperities; a scenario of slow slip is additionally supported by the detection of repeating events and the observation of episodes of slow epicentral migration (Kato & Nakagawa 2014). In such model, the lack of foreshocks and low seismicity rates in the region separating the two main patches (Fig. 10, top left), would correspond to the high coupling region, which experiences a stress accumulation until the main shock occurs. However, a further detailed analysis of continuous deformation data by Bedford *et al.* (2015) demonstrated that the transient GPS signal accompanying the foreshock sequence is
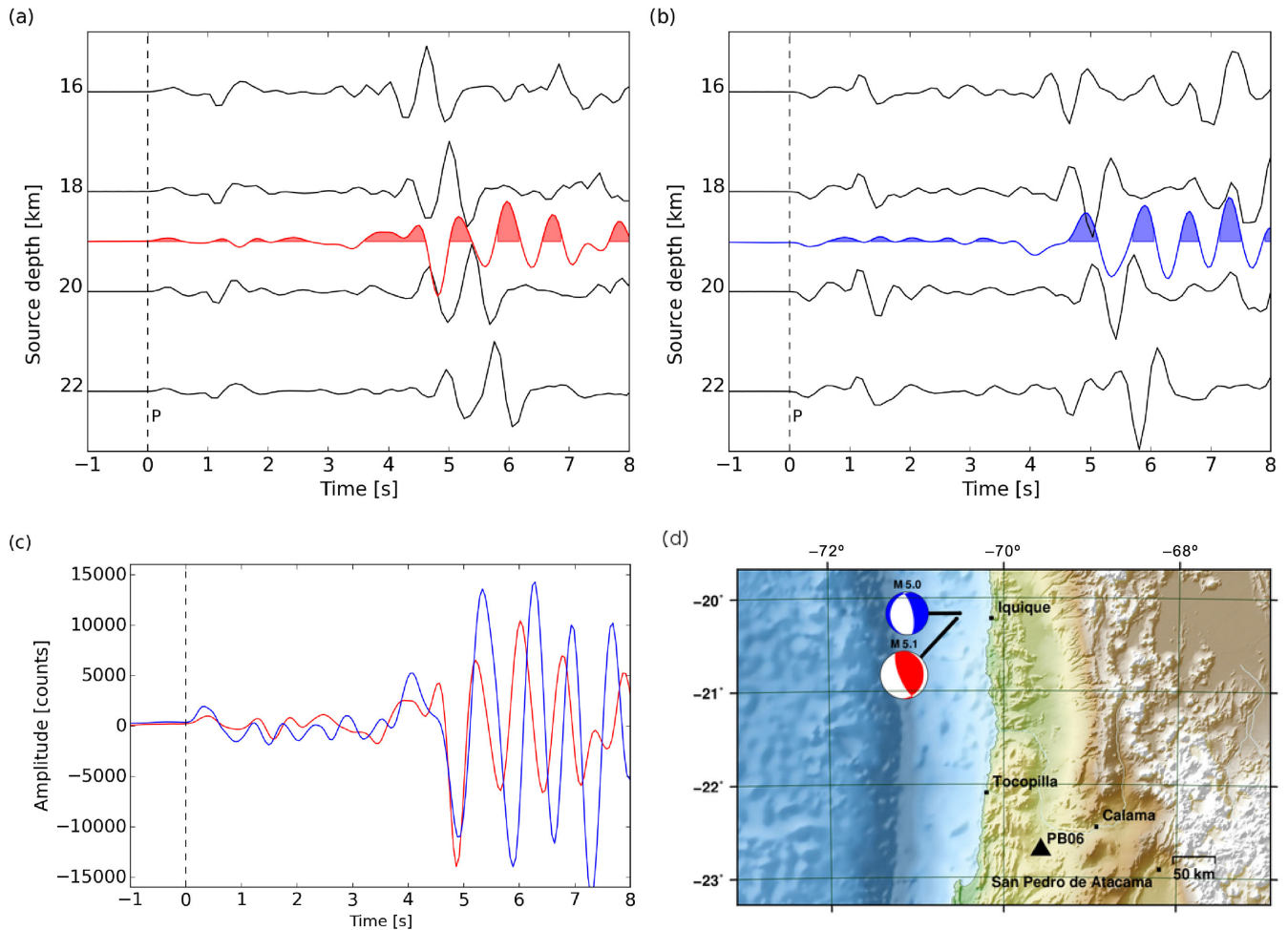
Figure 8. Depth estimation upon the modelling of vertical *P*-wave waveforms at station PB06 for two aftershocks with similar location and different focal mechanisms: an M_w 5.1 thrust faulting on 2014 April 5, 05:44:55 (a) and a normal faulting on 2014 April 11, 12:00:52 (b). Synthetic velocity waveforms (black lines) are plotted for different source depths, and compared to raw velocity data (coloured lines, plot (a) and red colour correspond to the thrust event, plot (b) and blue colour to the normal-faulting event). Data and synthetics are filtered between 0.1 and 1.6 Hz. The zero time reference corresponds to the arrival of the first P onset. The sea floor reflected P phase is observed starting at about 4 s. To highlight the waveform anticorrelation we compare (plot (c)) the signal of the thrust event (red line) with the inverted waveform of the normal-faulting event (blue line). Location of the events, focal mechanisms and reference PB06 stations are plotted in plot (d).

in large measure explained by seismic slip, and argued that even the observation of repeating event should not be considered as a strong argument for aseismic slip, considering that similar events occurred with a low regularity and rate in the two weeks preceding the main event, when the largest events in the foreshock sequence took place.

The main shock and largest aftershock also nucleated within these low coupled patches, but stress conditions permitted the rupture front to propagate through the locked zone, from the Northern and Southern side, respectively (Fig. 10, top centre). After the main shock, we observe that the spatial distribution of aftershocks is comparable to the foreshock activity, supporting the identification of local asperities, with the aftershocks slightly extending to deeper regions as consequence of weakening and stress redistribution induced by the main shock. After the main shock, when the accumulated stress was partially released, the central segment was locked again, as revealed by the returned conditions to low aftershock rate in that area (Fig. 10, top right). At the same time, focal mechanisms can be used to further extend the foreshock/main shock/aftershock rupture model to discuss stress rotation and to evaluate the stress released by the main shock (Fig. 10, bottom).

Our extensive MT inversion shows that focal mechanisms are dominated by thrust faulting, with focal plane geometries well fitting the slab orientation and dip (Hayes *et al.* 2012), extending previous results by Hayes et al. (2014) to smaller magnitudes. Few shallower thrust mechanisms are observed in the last weeks preceding the main shock, as first suggested by Ruiz *et al.* (2014). Our results show that thrust events were accompanied by less frequent normal faulting, which only occurred after the main shock. They appear to be localized close or slightly above the slab interface (Fig. 10, bottom right); a comparative depth analysis for different types of events showed that both thrust and normal faulting could occur within a very confined seismogenic region. The presence of normal-faulting events, so far not recognized in the Iquique sequence, was observed for previous large events in Chile (e.g. Fuenzalida *et al.* 2013; Sen *et al.* 2015). For larger magnitude thrust events, an outstanding normal-faulting aftershock seismicity has been observed, for example, for the Tohoku earthquake (e.g. Asano *et al.* 2011; Obana *et al.* 2012). Normal-faulting aftershocks in subduction environments can be attributed to a perturbation of the stress field and to its spatial heterogeneities. The stress inversion results could suggest a rotation
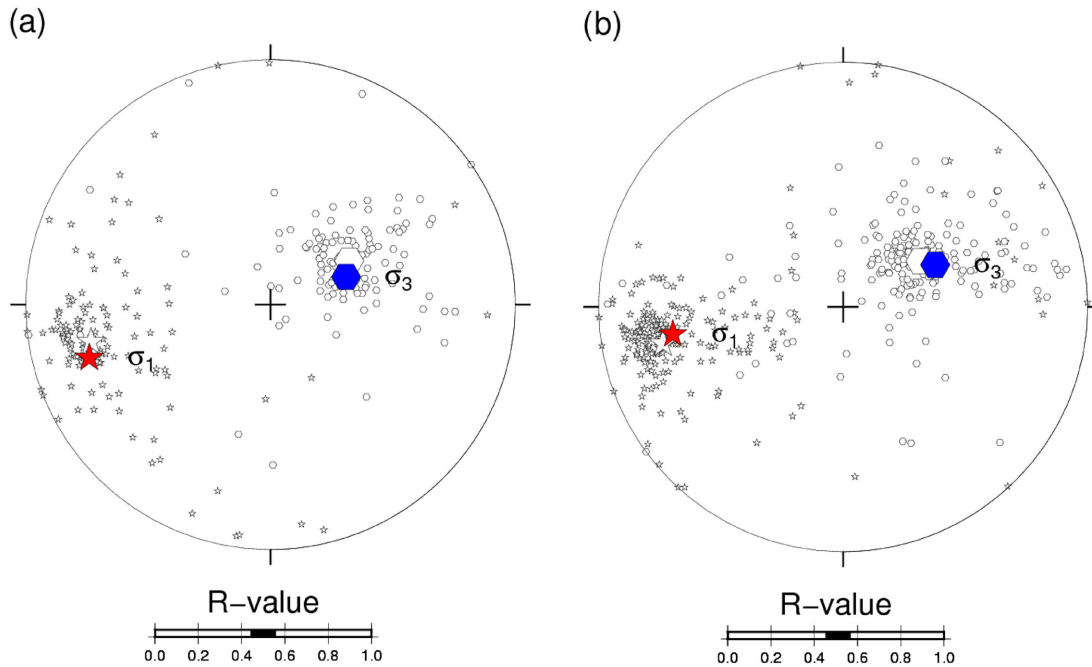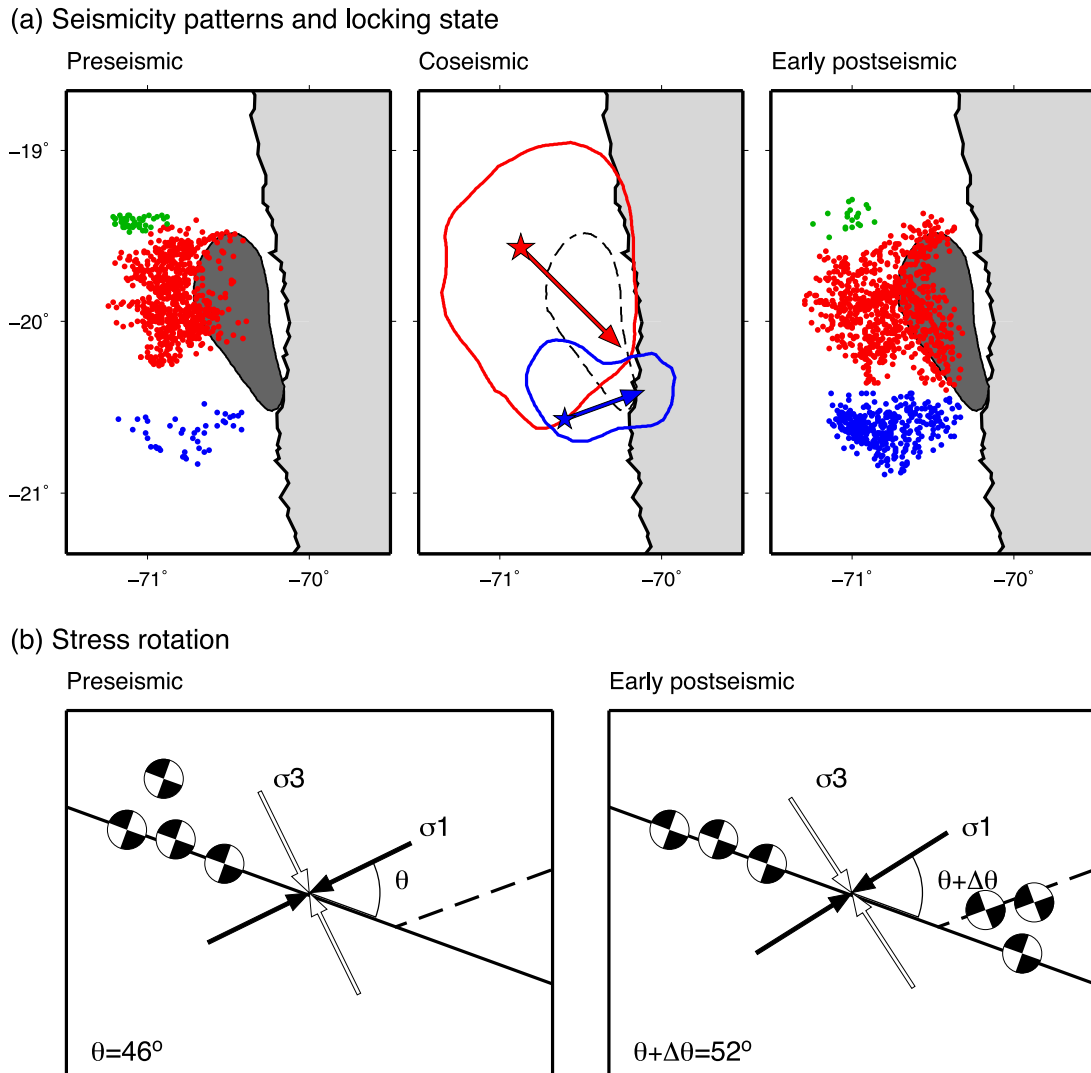
Figure 9. Stress inversion results from moment tensor solutions of the foreshock (a) and aftershock sequences (b). The orientations of the maximal (σ_1) and least (σ_3) compressive stress are projected (equal area) on the lower hemisphere. The *P*- and *T*-axes of the individual input moment tensors are indicated by open stars and diamonds, respectively. Large open symbols indicate the mean *P*- and *T*-axes orientations. The relative stress magnitude from the inversion is plotted in the horizontal scale below.

of the stress tensor (Fig. 9, bottom), in a similar way as proposed by Hardebeck (2012) for recent larger earthquakes, namely the Sumatra, Maule and Tohoku earthquakes. However, spatiotemporal evolutions of focal mechanisms of these foreshocks/aftershocks sequences present important differences. While for the Maule and the Iquique earthquakes normal-faulting aftershocks tended to be spatially localized and/or involved specific faults and were accompanied by a dominance of thrust events comparable to the foreshock sequences, the distributions of rupture types before and after the Tohoku earthquake were extremely different, with thrust mechanisms dominating the foreshocks and normal faulting predominant among aftershocks. Therefore, while a stress rotation is better resolved and seems unquestionable for the Tohoku event, the normal-faulting aftershocks for the considered Chilean events may either reflect a stress rotation or stress heterogeneities. The clustering results show that the family of thrust fault mechanisms preserves its geometry before and after the occurrence of the M_w 8.1 Iquique earthquake. This is not unexpected if they occur at the slab interface, where their orientation is controlled by the slab geometry and their rake by the plate convergence. In this condition, the foreshock activity would be favoured in both stress regimes derived independently from foreshocks and aftershocks. The change in the determined stress orientation is then controlled by the presence of normal-faulting aftershocks. We use the rotation of the stress tensor with respect to the slab orientation to infer the deviatoric stress released by the main shock, following eq. (9) in Hardebeck & Hauksson (2001). The stress rotation angle was quantified in 6.0°, upon the comparison of stress inversion results. The estimate of the angle of σ_1 with the slab orientation presents some uncertainty, since the main shock rupture occurs over a broad region of almost 100 km length, with variable dip at different depths. Here we assume as average slab dip the dip angle of the CMT inversion for the main shock (dip 24° east). Under these conditions, we estimate that the main shock has relieved 54 per cent of the pre-main shock devi-

atoric stress. However, this estimate would rise up to 85 per cent, if one chooses the slab dip according to the SLAB model (Hayes *et al.* 2012) at the centroid location. Beside the large uncertainty, the release of at least half of the deviatoric stress differs from the scenario hypothesized by Schurr *et al.* (2014), who assessed a significant moment deficit along the plate boundary after the Iquique earthquake, suggesting that part of the accumulated stress might have been relieved aseismically.

However, as mentioned before, the stress inversion results for the Iquique earthquake may also reflect the spatial heterogeneity of the stress conditions in the early post-seismic phase. To further investigate this hypothesis, we plot the distribution of the source types using a different graphical representation, first introduced by Frohlich (1992). In such representation (Fig. 11a), the striking of the focal mechanism is ignored and the focal mechanisms are plotted in a triangular diagram, where the coordinates are entirely controlled by the plunge of the pressure (*P*), tension (*T*) and null (*B*) axis. The interpretation of the triangular diagram is here facilitated by the colour scale, with red, blue and green corresponding to symmetric (i.e. 45° dipping) thrust and normal, and vertical strike-slip faulting, respectively. The Iquique sequence is characterized by low-angle thrust and few low-angle normal faulting, which map in the lower part of the diagram. The increased normal-faulting activity during the aftershock sequence can also be depicted with this representation. According to the spatial (Fig. 11b) distribution of the source type, we observe that normal-faulting events are mostly localized at the eastern edge of the aftershocks region; their centroid depths suggest they occur at the bottom of the overriding wedge, in a region which was untouched during the foreshock sequence. Their temporal evolution (Fig. 11c) shows that they are mostly active in the first 10–15 d after the main shock, and no longer active after middle April. Note that in Fig. 10c we plot the ratio among $\sin^2(\delta_P)$ and $(\sin^2(\delta_P) + \sin^2(\delta_T))$, where δ_i, with $i = T, P, B$ denotes the plunge of *T*-, *P*- and *B*-axes. The *y*-axis of the plot varies

(a) Seismicity patterns and locking state


(b) Stress rotation

Figure 10. A sketch of the foreshock preparation phase, main shock rupture and aftershock sequence, in the light of spatiotemporal evolution of seismicity rates, focal mechanisms and stress conditions. Top: during the foreshock sequence, seismicity spatially clusters in three small clusters (colour dots), with the largest red (Pisagua) and blue (Iquique) clusters separated by a region of high locking (dark area, after Schurr *et al.* 2014); the ruptures of main shock and largest aftershock nucleate within the Pisagua and Iquique clusters and propagate to the locked region (stars and arrows denote hypocentres and main rupture direction, after Schurr *et al.* 2014); the aftershocks are again mostly localized in correspondence to the original spatial clusters, and the central region is locked again. Bottom: at the same time, the orientation of σ_1 and σ_3 rotate from the pre-seismic phase to the post-seismic phase by 6° around a near-horizontal σ_2 axis, as revealed by the appearance of normal faulting (bottom right) along secondary faults (dashed line), beside dominant thrust mechanisms along the slab (thick line).

between pure normal (ratio $= 0$) and pure thrust (ratio $= 1$), while the effect of the *B*-axis plunge, largest for strike-slip events, is here neglected because we are interested in discussing only the temporal evolution of thrust versus normal-faulting components. In terms of the stress inversion, these findings reveal that the stress rotation inferred using the whole foreshock and aftershock seismicity is poorly constrained and hides significant spatial heterogeneities of focal mechanisms and stress orientation. Since the normal-faulting aftershocks occur in the eastern region, unaffected by the foreshock sequence, a comparison of the stress orientation limited to this region is hardly possible. A comparison of focal mechanisms in the western, shallower section of the slab and the overriding wedge, where both foreshocks and aftershock occurred (rectangular area in Fig. 11), indicates similar thrust mechanisms and no significant stress rotation. Even considering as robust the stress rotation inferred from foreshocks and aftershocks of the broader region, this

implies that the stress rotation would be localized to a smaller, eastern portion of the segment. The temporal evolution of rupture types shows that normal-faulting mechanisms are only acting in the first two weeks after the main shock. Therefore, even in the assumption of stress rotation, pre-seismic stress conditions seem to be quickly recovered already a couple of weeks after the main shock occurred, much quicker than for the Tohoku or Maule earthquakes (Hardebeck 2012).

8 CONCLUSIONS

A long-lasting seismic sequence struck the central segment of the former Northern Chile seismic gap offshore the cities of Iquique and Pisagua, leaving ~200 km long unbroken segments both towards north and south. The sequence presents peculiar features and
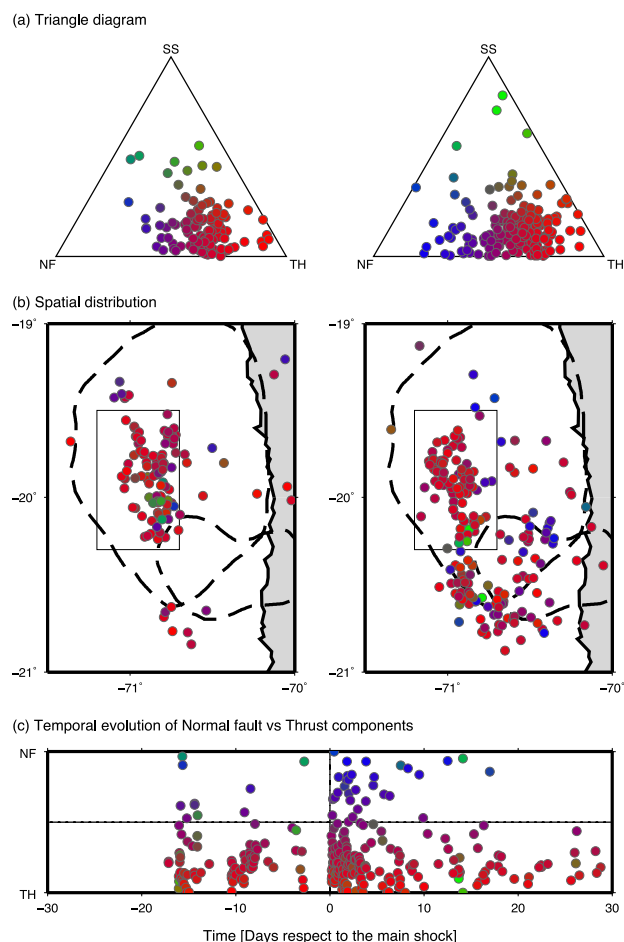
Figure 11. Comparison of the source type distribution among foreshocks (left) and aftershocks (right) upon the regional moment tensor inversion. (a) Comparison of source types, using a triangle diagram representations (Frohlich 1992) with red, blue and green corresponding to pure symmetric thrust, normal-faulting and strike-slip mechanisms, respectively. (b) Spatial distribution of the source types, the dashed lines provide reference to the rupture areas of the main shock and its largest aftershock (Schurr *et al.* 2014, see Fig. 10) and the thin solid black line denote a rectangular region with high seismicity both for during foreshock and aftershock sequence. (c) Temporal evolution of source types, plotting the balance between normal-faulting and thrust components, according to eq. (1).

allowed a comparison of foreshocks and aftershocks in terms of seismicity rates and families of focal mechanisms. The Iquique sequence lasted for months, the main shock only taking place after a long period of increased seismicity, and characterized by bursts of seismic activity at two main patches, with an overall increase of observed magnitudes since 2013 summer and until the M_w 8.1 main shock on 2014 April 1. Although a comparable foreshock seismicity was not observed for thrust earthquake in Northern Chile in the last decades, some foreshocks were reported before the 1933 earthquake, which struck at a location compatible with the main patch of the 2014 Iquique earthquake. This observation would indicate a peculiar behaviour of this section of the slab and suggests that similar foreshock activities may also precede future large earthquakes in the region and that the main patch could correspond to a repeatedly activated asperity. The area affected by the foreshock activity matched

the spatial extension of the aftershock sequence, and controlled the final lateral extension of the main earthquakes finite rupture, which was constrained to a subsegment of the seismic gap. However, the aftershocks additionally activated deeper portions of the slab interface. A newly proposed method based on the stacking of normalized coherence matrices for multiple events, which accounts for location uncertainties, was able to detect temporal changes of the spatial distribution of seismicity rates, which is here evaluated for different time frames throughout the sequence. An MT inversion was performed for more than 300 events, revealing dominant thrust focal mechanisms in the foreshock and aftershock activity. The application of a focal mechanism clustering algorithm revealed that the main orientation of the thrust mechanisms remain unchanged before and after the main shock. However, during the aftershock sequence, thrust events were accompanied by sporadic and weaker normal-faulting earthquakes. They are mostly localized at the eastern edge of the seismicity cloud, originating in the vicinity of thrust events at or slightly above the slab interface, possibly along secondary faults in the overriding wedge. The analysis of focal mechanisms distributions in the two main seismicity patches, the Pisagua and Iquique clusters, reveals homogeneous thrust focal mechanism orientations, with no spatial nor temporal variations neither in the rupture plane geometry, nor in the rake direction. Whereas the plane geometry of thrust events is constrained along the whole sequence to the slab geometry, the lack of significant change in the rake angles at the Iquique and Pisagua clusters suggests a negligible lateral stress heterogeneity. Assuming a spatially homogeneous stress condition, a stress rotation of about 6° has been inferred by the comparison of foreshock and aftershock focal mechanisms. Beside this small rotation angle, the temporal evolution of the stress orientation would suggest that the 2014 April 1, main shock relieved most than half of the accumulated deviatoric stress. However, a more careful analysis of the spatial and temporal distributions of the focal mechanisms indicates that a stress rotation can only be hypothesized for a limited portion of the slab interface, and that pre-seismic stress conditions are restored already in 2014 mid-April. The neighbouring northern and southern segments of the former Northern Chile seismic gap remain unbroken and can potentially host large magnitude events. The recent seismic sequence has locally reduced the stress accumulated at sections of the Iquique–Pisagua segment, but a future single rupture of the entire Northern Chile seismic gap remains a possible scenario.

REFERENCES

Angelier, J., 2002. Inversion of earthquake focal mechanisms to obtain the seismotectonic stress—a new method free of choice among nodal lines, *Geophys. J. Int.,* **150,** 588–609.

Asano, Y. *et al.*, 2011. Spatial distribution and focal mechanisms of aftershocks of the 2011 off the Pacific coast of Tohoku earthquake, *Earth Planets Space,* **63**(7), 669–673.

Bassin, C., Laske, G. & Masters, G., 2000. The current limits of resolution for surface wave tomography in North America, *EOS, Trans. Am. geophys. Un.,* **81**(48), Fall Meet. Suppl., Abstract S12A-03.

Bedford, J., Moreno, M., Schurr, B., Bartsch, M. & Oncken, O., 2015. Investigating the final seismic swarm before the Iquique-Pisagua 2014 M_w 8.1 by comparison of continuous GPS and seismic foreshock data, *Geophys. Res. Lett.,* **42**(10), 3820–3828.

Béjar-Pizarro, M., Socquet, A., Armijo, R., Carrizo, D., Genrich, J. & Simons, M., 2013. Andean structural control on interseismic coupling in the North Chile subduction zone, *Nature Geosci.,* **6,** 462–467.

Bilek, S.L. & Ruff, L.J., 2002. Analysis of the 23 June 2001 M_w 8.4 Peru underthrusting earthquake and its aftershocks, *Geophys. Res. Lett.,* **29**(20), doi:10.1029/2002GL015543.

Bouchon, M., Durand, V., Marsan, D., Karabulut, H. & Schmittbuhl, J., 2013. The long precursory phase of most large interplate earthquakes, *Nature Geosci.,* **6,** 299–302.

Bürgmann, R., 2014. Warning signs of the Iquique earthquake, *Nature,* **512,** 258–259.

Cesca, S., Heimann, S., Stammler, K. & Dahm, T., 2010. Automated procedure for point and kinematic source inversion at regional distances, *J. geophys. Res.,* **115,** B06304, doi:10.1029/2009JB006450.

Cesca, S., Rohr, A. & Dahm, T., 2013. Discrimination of induced seismicity by full moment tensor inversion and decomposition, *J. Seismol.,* **17**(1), 147–163.

Cesca, S., Sen, A.T. & Dahm, T., 2014. Seismicity monitoring by cluster analysis of moment tensors, *Geophys. J. Int.,* **196**(3), 1813–1826.

Comte, D. & Pardo, M., 1991. Reappraisal of great historical earthquakes in the Northern Chile and Southern Peru seismic gaps, *Nat. Hazards,* **4,** 23–44.

Delouis, B. *et al.*, 1997. The $M_w = 8.0$ Antofagasta (Northern Chile) Earthquake of 30 July 1995. A precursor to the end of the large 1877 gap, *Bull. seism. Soc. Am.,* **87**(2), 427–445.

Delouis, B., Pardo, M., Legrand, D. & Monfret, T., 2009. The M_w 7.7 Tocopilla earthquake of 14 November 2007 at the southern edge of the Northern Chile seismic gap: rupture in the deep part of the coupled plate interface, *Bull. seism. Soc. Am.,* **99**(1), 87–94.

Dodge, D.A., Beroza, G.C. & Ellsworth, W.L., 1995. Foreshock sequence of the 1992 Landers, California, earthquake and its implications for earthquake nucleation, *J. geophys. Res.,* **100,** 9865–9880.

Dodge, D.A., Beroza, G.C. & Ellsworth, W.L., 1996. Detailed observations of California foreshock sequences: implications for the earthquake initiation process. *J. geopyhs. Res.,* **101**(B10), 22 371–22 392.

Dorbath, L., Cisternas, A. & Dorbath, C., 1990. Quantitative assessment of great earthquakes in Peru. *Bull. seism. Soc. Am.,* **80,** 551–576.

Drew, J., White, R.S., Tilmann, F. & Tarasewicz, J., 2013. Coalescence microseismic mapping, *Geophys. J. Int.,* **195**(3), 1773–1785.

Dura, T., Cisternas, M., Horton, B.P., Ely, L.L., Nelson, A.R., Wesson, R.L. & Pilarczyk, J.E., 2015. Coastal evidence for Holocene subduction-zone earthquakes and tsunamis in central Chile, *Quat. Sci. Rev.,* **113,** 93–111.

Engdahl, E.R. & Villaseñor, A., 2002. Global seismicity: 1900–1999, in *International Handbook of Earthquake and Engineering Seismology, Part A, chap. 41*, pp. 665–690, eds Lee, W.H.K., Kanamori, H., Jennings, P.C. & Kisslinger, C., Academic Press.

Frohlich, C., 1992. Triangle diagrams: ternary graphs to display similarity and diversity of earthquake focal mechanisms, *Phys. Earth planet. Inter.,* **75,** 193–198.

Fuenzalida, A., Schurr, B., Lancieri, M., Sobiesiak, M. & Madariaga, R., 2013. High-resolution relocation and mechanism of aftershocks of the 2007 Tocopilla (Chile) earthquake. *Geophys. J. Int.,* **194**(2), 1216–1228.

Gephart, J.W., 1990. Stress and the direction of slip on faults, *Tectonics,* **9**(4), 845–858.

Gephart, J.W. & Forsyth, D.W., 1984. An improved method for determining the regional stress tensor using earthquake focal mechanism data: application to the San Fernando earthquake sequence, *J. geophys. Res.,* **89,** 9305–9320.

GFZ German Research Centre for Geosciences & Institut des Sciences de l'Univers-Centre National de la Recherche CNRS-INSU, 2006. IPOC Seismic Network. Integrated Plate boundary Observatory Chile—IPOC. Other/Seismic Network, doi:10.14470/PK615318.

Grigoli, F., Cesca, S., Vassallo, M. & Dahm, T., 2013. Automated seismic event location by traveltime stacking: an application to mining induced seismicity, *Seismol. Res. Lett.,* **84**(4) 666–677.

Grigoli, F., Cesca, S., Amoroso, O., Emolo, A., Zollo, A. & Dahm, T., 2014. Automated seismic event location by waveform coherence analysis, *Geophys. J. Int.,* **196**(3), 1742–1753.

Hardebeck, J.L., 2012. Coseismic and postseismic stress rotations due to great subduction zone earthquakes, *Geophys. Res. Lett.,* **39**(21), doi:10.1029/2012GL053438.

Hardebeck, J.L. & Hauksson, E., 2001. Crustal stress field in southern California and its implications for fault mechanics, *J. geophys. Res.,* **106**(B10), 21 859–21 882.

Hayes, G.P., Wald, D.J. & Johnson, R.L., 2012. Slab1.0: a three-dimensional model of global subduction zone geometries, *J. geophys. Res.,* **117,** B01302, doi:10.1029/2011JB008524.

Hayes, G.P. *et al.*, 2014. Continuing megathrust earthquake potential in Chile after the 2013 Iquique earthquake, *Nature,* **512,** 295–298.

Heimann, S., 2011. A robust method to estimate kinematic earthquake source parameters, *PhD thesis,* University of Hamburg, Hamburg, Germany.

Helmstetter, A. & Sornette, D., 2003. Foreshocks explained by cascades of triggered seismicity, *J. geophys. Res.*, **108**(B10), 2457, doi:10.1029/2003JB002409.

Jones, L.M. & Molnar, P., 1976. Frequency of foreshocks, *Nature* **262,** 677–679.

Kagan, Y.Y., 1991. 3-D rotation of double-couple earthquake sources, *Geophys. J. Int.,* **106,** 709–716.

Kanamori, H., 1981. The nature of seismicity patterns before large earthquakes, in *Earthquake Prediction*, pp. 1–19, eds Simpson, D.W. & Richards, P.G., American Geophysical Union.

Kato, A. & Nakagawa, S., 2014. Multiple slow-slip events during a foreshock sequence of the 2014 Iquique, Chile M_w 8.1 earthquake, *Geophys. Res. Lett.,* **41**(15), 5420–5427.

Lomnitz, C., 2004. Major earthquakes of Chile: a historical survey, 1535–1960, *Seismol. Res. Lett.*, **75**(3), 368–378.

Maghsoudi, S., Hainzl, S., Cesca, S., Dahm, T. & Kaiser, D., 2014. Identification and characterization of growing large-scale en-echelon fractures in a salt mine, *Geophys. J. Int.,* **196**(2), 1092–1105.

Malgrange, M. & Madariaga, R., 1983. Complex distribution of large thrust and normal fault earthquakes in the Chilean subduction zone, *Geophys. J. R. astr. Soc.,* **73,** 489–505.

Maury, J., Cornet, F.H. & Dorbath, L., 2013. A review of methods for determining stress fields from earthquake focal mechanisms: application to the Sierentz 1980 seismic crisis (Upper Rhine graben), *Bull. Soc. Geol. France,* **184**(4–5), 319–334.

Meng, L., Huang, H., Bürgmann, R., Ampuero, J.P. & Strader, A., 2015. Dual megathrust slip behaviors of the 2014 Iquique earthquake sequence, *Earth planet. Sci. Lett.,* **411,** 177–187.

Metois, M. *et al.*, 2013. Revisiting the North Chile seismic gap segmentation using GPS-derived interseismic coupling, *Geophys. J. Int.,* **194,** 1283–1294.

Michael, A.J., 1984. Determination of stress from slip data: faults and folds, *J. geophys. Res.,* **89,** 11 517–11 526.

Michael, A.J., 1987. Use of focal mechanism to determine stress: a control study, *J. Geophys. Res.,* **92,** 357–368.

Mignan, A., 2012. Seismicity precursors to large earthquakes unified in a stress accumulation framework, *Geophys. Res. Lett.,* **39,** L21308, doi:10.1029/2012GL053946.

Mignan, A., 2014. The debate on the prognostic value of earthquake foreshocks: a meta-analysis, *Sci. Rep.,* **4,** 4099, doi:10.1038/srep04099.

Nishenko, S.P., 1985. Seismic potential for large and great intraplate earthquakes along the Chilean and southern Peruvian margins of South America: a quantitative reappraisal, *J. geophys. Res.,* **90,** 3589–3615.

Norabuena, E., Leffler-Griffin, L., Mao, A., Dixon, T., Stein, S., Selwyn Sacks, I., Ocola, L. & Ellis, M., 1998. Space geodetic observations of Nazca-South America convergence across the central Andes, *Science,* **279**(5349), 358–362.

Obana, K. *et al.*, 2012. Normal-faulting earthquakes beneath the outer slope of the Japan Trench after the 2011 Tohoku earthquake: implications for the stress regime in the incoming Pacific plate, *Geophys. Res. Lett.,* **39,** L00G24, doi:10.1029/2011GL050399.

Pritchard, M.E., Norabuena, E.O., Ji, C., Boroscheck, R., Comte, D., Simons, M., Dixon, T.H & Rosen, P.A., 2007. Geodetic, teleseismic, and strong motion constraints on slip from recent southern Peru subduction zone earthquakes, *J. geophys. Res.,* **112,** B03307, doi:10.1029/2006JB004294.

Reinhardt, J., 2007. Inversion for local stress field inhomogeneities, *PhD thesis,* Institute of Geophysics, University of Hamburg, Hamburg, Germany.

Ruegg, J.C. *et al.*, 1996. The $M_W = 8.1$ Antofagasta (North Chile) Earthquake of July 30, 1995: first results from teleseismic and geodetic data, *Geophys. Res. Lett.,* **23,** 917–920.

Ruiz, S. *et al.*, 2014. Intense foreshocks and a slow slip event preceded the 2014 Iquique M_w 8.1 earthquake, *Science,* **345**(6201), 1165–1169.

Schurr, B. *et al.*, 2009. The International Plate Boundary Observatory Chile (IPOC) in the Northern Chile seismic gap, *Geophys. Res. Abstr.,* **11,** abstract EGU2009-11040.

Schurr, B., Asch, G., Rosenau, M., Wang, R., Oncken, O., Barrientos, S., Salazar, P. & Villotte, J.-P., 2012. The 2007 M7.7 Tocopilla Northern Chile earthquake sequence: implications for along-strike and downdip rupture segmentation and megathrust frictional behaviour, *J. geophys. Res.,* **117,** B05305, doi:10.1029/2011JB009030.

Schurr, B. *et al.*, 2014. Gradual unlocking of the plate boundary controlled the initiation of the 2014 Iquique earthquake, *Nature,* **512**(7514), 299–302.

Sen, A.T., Heimann, S., Cesca, S., Lange, D., Dahm, T. & Tilmann, F., 2015. Systematic changes of earthquake rupture with depth: a case study from the 2010 M_w 8.8 Maule, Chile, earthquake aftershock sequence, *Bull. seism. Soc. Am.,* **105**(5), 2468–2479.

Sobiesiak, M., 2000. Fault plane structure of the Antofagasta, Chile Earthquake of 1995, *Geophys. Res. Lett.,* **27**(4), 581–584.

Wang, R., 1999. A simple orthonormalization method for stable and efficient computation of Green's functions, *Bull. seism. Soc. Am.,* **89**(3), 733–741.

Wessel, P., Smith, W.H.F., Scharroo, R., Luis, J.F. & Wobbe, F., 2013. Generic mapping tools: improved version released, *EOS, Trans. Am. geophys. Un.,* **94,** 409–410.